# Wideband MIMO Systems: Signal Design for Transmit Beampattern Synthesis

Hao He, *Student Member, IEEE*, Petre Stoica, *Fellow, IEEE*, and Jian Li, *Fellow, IEEE*

***Abstract*—The usage of multi-input multi-output (MIMO) systems such as a MIMO radar allows the array elements to transmit different waveforms freely. This waveform diversity can lead to flexible transmit beampattern synthesis, which is useful in many applications such as radar/sonar and biomedical imaging. In the past literature most attention was paid to receive beampattern design due to the stringent constraints on waveforms in the transmit beampattern case. Recently progress has been made on MIMO transmit beampattern synthesis but mainly only for narrowband signals. In this paper we propose a new approach that can be used to efficiently synthesize MIMO waveforms in order to match a given wideband transmit beampattern, i.e., to match a transmit energy distribution in both space and frequency. The synthesized waveforms satisfy the unit-modulus or low peak-to-average power ratio (PAR) constraints that are highly desirable in practice. Several examples are provided to investigate the performance of the proposed approach.**

***Index Terms*—Multi-input multi-output (MIMO), signal synthesis, transmit array beampattern, wideband.**

## I. Introduction

ANTENNA array beampattern design has been a well-studied topic and there is a considerable literature available from the classic analytical design [1]–[5] to the more recent works that resort to numerical optimization [6]–[10]. The predominant setting used in the literature is the *receive* beampattern design, which refers to designing weights for the received signal so that the signal component impinging from a particular direction is reinforced while those from other directions are attenuated, a way in which certain signal properties (e.g., the signal power or direction-of-arrival) can be estimated. Such a problem usually boils down to the design of a finite-impulse-response (FIR) filter in the narrowband case or a set of FIR filters in the wideband case.

The *transmit* beampattern design, on the other hand, refers to designing the probing signals to approximate a desired transmit beampattern (i.e., an energy distribution in space and frequency). It has been often stated that the receive and transmit beampattern designs are essentially identical, which is partly true in the sense that the two scenarios bear similar problem formulations and that the FIR filter taps obtained in a receive pattern design can be used theoretically as the transmit signal to achieve the same pattern. In practice, however, the transmit beampattern design problem appears to be much harder because of the energy and peak-to-average power ratio (PAR) constraints on transmit waveforms. In particular, a digital-to-analog converter scales the signal by the maximum allowable amplitude and a saturated power amplifier works well only when the signal is constant-modulus [11], [12]. If the transmitted signals have largely varying amplitudes, we risk energy-loss or even signal distortion. As a result, the transmit beampattern design is subject to the constraint that the transmit waveforms are unit-modulus or have low PARs. On the contrary in the receive beampattern design, the FIR taps can take any values, although certain easy-to-meet constraints (e.g., the symmetry of the filter coefficients) are usually imposed. Therefore, except in a few simple situations such as the phased array case, transmit beampattern design should be treated differently from the prevalent receive beampattern design.

The *narrowband* transmit beampattern design problem has been addressed in the MIMO radar area, e.g., in [13]–[16], and in biomedical imaging, e.g., in [17]. Most of the proposed methods first relate the desired beampattern to the cross correlations between the transmit signals, then aim to design the signal covariance matrix and finally synthesize the actual signals (see, e.g., [16]). In the *wideband* case, similar approaches have been proposed to design the power spectral density matrix (see, e.g., [9]), but no signals have been synthesized due to the difficulty of imposing the unit-modulus or PAR constraints.

In this paper we propose a new algorithm named Wideband Beampattern Formation via Iterative Techniques (WBFIT) to design unimodular or low-PAR sequences for transmit beampattern synthesis in wideband MIMO systems. We do not formulate the problem in terms of the transmit spectral density matrix (as was done in [9]), but instead directly link the beampattern to the signals through their Fourier transform. The design criterion is formulated in Section II, which is followed by the algorithm description in Section III. Simulation examples are shown in Section IV and concluding remarks are given in Section V.

Manuscript received March 04, 2010; revised July 01, 2010, September 22, 2010; accepted November 01, 2010. Date of publication November 11, 2010; date of current version January 12, 2011. The associate editor coordinating the review of this manuscript and approving it for publication was Dr. Dennis Morgan. This work was supported in part by the Office of Naval Research (ONR) under Grants N00014-09-1-0211 and N00014-10-1-0054, the National Science Foundation (NSF) under Grant CCF-0634786, the U.S. Army Research Laboratory and the U.S. Army Research Office under Grants W911NF-07-1-0450 and W911NF-11-C-0020, the Swedish Research Council (VR), and the European Research Council (ERC). The views and conclusions contained herein are those of the authors and should not be interpreted as necessarily representing the official policies or endorsements, either expressed or implied, of the U.S. Government. The U.S. Government is authorized to reproduce and distribute reprints for Governmental purposes notwithstanding any copyright notation thereon.

H. He and J. Li are with the Department of Electrical and Computer Engineering, University of Florida, Gainesville, FL 32611 USA (e-mail: haohe@ufl.edu; li@dsp.ufl.edu).

P. Stoica is with the Department of Information Technology, Uppsala University, SE-75105 Uppsala, Sweden (e-mail: ps@it.uu.se).

Color versions of one or more of the figures in this paper are available online at http://ieeexplore.ieee.org.

Digital Object Identifier 10.1109/TSP.2010.2091410

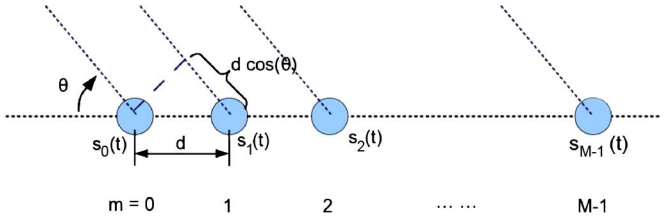


Fig. 1. The ULA array configuration.

Throughout the discussion we use bold lowercase/uppercase letters to denote vectors/matrices, respectively. The vector/matrix elements are indexed from zero. $(\cdot)^H$ indicates vector/matrix conjugate transpose and $(\cdot)^T$ indicates transpose. $\arg(x)$ denotes the phase of $x$, $\|\cdot\|$ the vector Euclidean norm and $\lfloor x \rfloor$ the largest integer less than or equal to $x$.

## II. Problem Formulation

We focus on far-field beampattern synthesis for uniform linear arrays (ULA) as illustrated in Fig. 1. Suppose that there are $M$ linearly spaced isotropic array elements and the inter-element spacing is $d$. The signal transmitted by the $m^{\text{th}}$ element is denoted as $s_m(t)$. Consider the beampattern in the far field at angle $\theta$ ($0^\circ \le \theta \le 180^\circ$) measured with respect to (w.r.t.) the array plane. It is easy to see that the time delay between two neighboring elements is $d\cos\theta/c$, where $c$ is the speed of wave propagation (e.g., electromagnetic waves for radar or sound waves for sonar). We let $s_m(t) = x_m(t)e^{j2\pi f_c t}$ where $f_c$ is the carrier frequency and $x_m(t)$ is the baseband signal whose spectral support is assumed to be included in the interval $[-(B/2), B/2]$.

By using the above notation, the resulting far-field signal at angle $\theta$ can be written as

$$z_\theta(t) = \sum_{m=0}^{M-1} s_m\left(t - \frac{md\cos\theta}{c}\right) = \sum_{m=0}^{M-1} x_m\left(t - \frac{md\cos\theta}{c}\right) e^{j2\pi f_c\left(t - \frac{md\cos\theta}{c}\right)}. \quad (1)$$

Suppose that the time support of $x_m(t)$ is $[0, \tau]$. Then the Fourier transform of $x_m(t)$ is given by

$$y_m(f) = \int_0^\tau x_m(t)e^{-j2\pi ft}\,dt, \quad f \in \left[-\frac{B}{2}, \frac{B}{2}\right] \quad (2)$$

and the inverse Fourier transform is given accordingly by

$$x_m(t) = \int_{-B/2}^{B/2} y_m(f)e^{j2\pi ft}\,df. \quad (3)$$

Substituting (3) into (1) yields

$$z_\theta(t) = \int_{-B/2}^{B/2} Y(\theta, f)e^{j2\pi(f+f_c)t}\,df \quad (4)$$

where

$$Y(\theta, f) = \sum_{m=0}^{M-1} y_m(f)e^{-j2\pi(f+f_c)\frac{md\cos\theta}{c}}. \quad (5)$$

Consequently, the beampattern at spatial angle $\theta$ and frequency $f + f_c$ can be defined as

$$P(\theta, f+f_c) = |Y(\theta, f)|^2 = \left|\mathbf{a}^H(\theta, f)\mathbf{y}(f)\right|^2, \quad f \in \left[-\frac{B}{2}, \frac{B}{2}\right] \quad (6)$$

where

$$\mathbf{a}(\theta, f) = \left[1 \;\; e^{j2\pi(f+f_c)\frac{d\cos\theta}{c}} \;\; \cdots \;\; e^{j2\pi(f+f_c)\frac{(M-1)d\cos\theta}{c}}\right]^T \quad (7)$$

and

$$\mathbf{y}(f) = [y_0(f) \;\; y_1(f) \;\; \cdots \;\; y_{M-1}(f)]^T. \quad (8)$$

Our problem can be stated as designing a set of signals $\{x_m(t)\}_{m=0}^{M-1}$ (band-limited to $[-B/2, B/2]$) so that the beampattern $P(\theta, f + f_c)$ in (6) matches a desired one. In the sequel, the baseband frequency range $[-B/2, B/2]$ is explicitly used most of the time.

Digital signal processing techniques deal with the sampled signal

$$x_m(n) \triangleq x_m(t = nT_s), \quad n = 0, \ldots, N-1 \quad (9)$$

where $T_s$ is the symbol period that satisfies $T_s = 1/B$ and $N = \lfloor \tau/T_s \rfloor$. Then (2) becomes (by a slight abuse of notation)

$$y_m(fT_s) = T_s \sum_{n=0}^{N-1} x_m(nT_s)e^{-j2\pi fnT_s}, \quad f \in \left[-\frac{B}{2}, \frac{B}{2}\right]. \quad (10)$$

Since the interval for $fT_s$ is $[-0.5, 0.5]$, it is enough to consider the discrete Fourier transform (DFT) of $x_m(n)$

$$y_m(p) = \sum_{n=0}^{N-1} x_m(n)e^{-j2\pi\frac{np}{N}}, \quad p = -\frac{N}{2}, \ldots, 0, \ldots, \frac{N}{2} - 1 \quad (11)$$

where $N$ was assumed to be even ($p$ will be from $-(N-1)/2$ to $(N-1)/2$ if $N$ is odd). Note that in (11) we have dropped the multiplicative constant $T_s$ from (10) since the scaling of $\{y_m(p)\}$ does not affect the proposed approach (see the discussions following (30) in Section III).

Similarly to the frequency grid above, we also divide the spatial angle interval $[0^\circ, 180^\circ]$ using a grid with points denoted as $\{\theta_k\}_{k=1}^K$. For notational simplicity, let

$$\mathbf{a}_{kp} = \mathbf{a}\left(\theta_k, \frac{p}{NT_s}\right) \quad (\text{see } (7)) \quad (12)$$

and

$$\mathbf{y}_p = [y_0(p) \;\; y_1(p) \;\; \cdots \;\; y_{M-1}(p)]^T \quad (\text{see } (11)). \quad (13)$$

Note that $\{\mathbf{y}_p\}_{p=-N/2}^{N/2-1}$ represents the DFT (element-wise) of

$$\mathbf{x}(n) = [x_0(n) \;\; x_1(n) \;\; \cdots \;\; x_{M-1}(n)]^T, \quad n = 0, \ldots, N-1. \quad (14)$$

Then it follows from (6) that the beampattern can be expressed on the discrete angle-frequency grid as

$$P_{kp} = \left|\mathbf{a}_{kp}^H \mathbf{y}_p\right|^2. \tag{15}$$

Letting $d_{kp}$ denote the desired beampattern, we seek to solve the following beampattern matching problem:

$$\min_{\{x_m(n)\}} \sum_{k=1}^{K} \sum_{p=-N/2}^{N/2-1} \left[d_{kp} - \left|\mathbf{a}_{kp}^H \mathbf{y}_p\right|\right]^2$$
$$\text{subject to } \mathrm{PAR}(\mathbf{x}_m) \le \rho, \quad m = 0, \ldots, M-1 \tag{16}$$

where $\rho \ge 1$ is a predefined threshold and the PAR of the $m^{\text{th}}$ sequence is defined as

$$\mathrm{PAR}(\mathbf{x}_m) = \frac{\max_n \left|x_m(n)\right|^2}{\frac{1}{N}\sum_{n=0}^{N-1} \left|x_m(n)\right|^2}. \tag{17}$$

[Note that in (16) the minimizer $\{x_m(n)\}$ comes into the criterion through its Fourier transform $\{\mathbf{y}_p\}$.] Without loss of generality, we impose the following energy-constraint:

$$\sum_{n=0}^{N-1} \left|x_m(n)\right|^2 = N, \quad m = 0, \ldots, M-1. \tag{18}$$

In this way, $\rho = 1$ is equivalent to the unit-modulus constraint, i.e., $|x_m(n)| = 1$.

The optimization problem in (16) is nonconvex (and thus difficult in general) because of the PAR constraint. This nonconvexity can be easily seen in the case of $\rho = 1$: each $x_m(n)$ can only take values from the unit-circle, which is not a convex set. Furthermore, exhaustive search is not practical here because we have $MN$ continuous variables (i.e., the phases) in $[0, 2\pi)$ when $\rho = 1$ and have an even larger variable space when $\rho > 1$. Stochastic optimization algorithms such as the simulated annealing also turn out to be too computationally expensive. In Section III, an efficient cyclic algorithm will be proposed to search for the local minimum of (16).

*Remark:* The paper [9] considers the transmit beampattern given by

$$\mathbf{a}^H(\theta, f)\mathbf{\Phi}(f)\mathbf{a}(\theta, f) \tag{19}$$

where $\mathbf{\Phi}(f)$ is the power spectral density matrix of $\mathbf{x}(n)$. (19) can be interpreted as the average of our expression (6) over the ensemble of realizations of the signal. Therefore (19) is not directly related to the finite-length power, unlike (6) which is the power we really want to control. Note that in (19), $\mathbf{\Phi}(f)$ has typically a full rank, whereas in (6) the periodogram $\mathbf{y}(f)\mathbf{y}(f)^H$ has rank one. Hence there are essential differences between (6) and (19). Furthermore, the algorithm proposed in [9] is computationally expensive so that very few frequency bins are considered (such as 5); in fact the ratio between the $B$ and $f_c$ used in [9] is only 5% whereas for the wideband scenario the ratio is typically assumed to be larger than 10% (see e.g., [18]). Finally, and likely most importantly, [9] does not discuss how to design unit-modulus or low PAR signals that synthesize the desired $\mathbf{\Phi}(f)$. ■

*Remark:* Note that $\{x_m(n)\}$ is typically related to $\{x_m(t)\}$ through pulse shaping:

$$x_m(t) = \sum_{n=0}^{N-1} x_m(n) p(t - nT_s), \quad m = 0, \ldots, M-1 \tag{20}$$

where $p(t)$ is the pulse. The spectrum of the baseband signal $x_m(t)$ would be confined to $[-B/2, B/2]$ only if $p(t)$ were a perfect Nyquist shaping pulse (i.e., a sinc function which is centered at 0 and has the first zero-crossing at $T_s$). The use of any practical shaping pulse such as a (truncated) raised cosine [19] will result in a distortion of the spectrum of $x_m(t)$, as well as a leakage of the spectrum outside the desired range $[-B/2, B/2]$; these facts make (6) and (15) only approximately equivalent. We will examine this discrepancy in an example in Section IV.

In addition, note that the narrowband MIMO transmit beampattern design is just a special case of the wideband problem considered here and that the receive beampattern design can be given a similar formulation which, however, differs in important ways from the transmit problem; see Appendix A and B for more details on these aspects. ■

## III. The Proposed Design Methodology

Minimization of the criterion in (16) directly w.r.t. $\{x_m(n)\}$ appears to be a difficult task (unless the matrix $[\mathbf{a}_{1p} \ \cdots \ \mathbf{a}_{Kp}]$ turns out to be semi-unitary for each value of $p$, which is hardly true in general). For this reason we adopt a two-stage design approach:

Stage 1: First we solve (16) w.r.t. $\{\mathbf{y}_p\}$ considered to be general vectors in $\mathbb{C}^{M\times 1}$.

Stage 2: Then we fit the DFT of $\{\mathbf{x}(n)\}$ to the so-obtained $\{\mathbf{y}_p\}$, subject to (s.t.) the enforced PAR constraint on $\{\mathbf{x}(n)\}$.

### A. Stage 1

For a generic term $\left[d - |\mathbf{a}^H\mathbf{y}|\right]^2$ of (16) it holds that $(d \ge 0)$

$$\begin{aligned}\min_{\phi} &\left|de^{j\phi} - \mathbf{a}^H\mathbf{y}\right|^2 \\ &= \min_{\phi} \left\{d^2 + \left|\mathbf{a}^H\mathbf{y}\right|^2 - 2\mathrm{Re}\left[d|\mathbf{a}^H\mathbf{y}|\cos\left(\phi - \arg(\mathbf{a}^H\mathbf{y})\right)\right]\right\} \\ &= \left[d - |\mathbf{a}^H\mathbf{y}|\right]^2 \quad \left(\text{for } \phi = \arg\{\mathbf{a}^H\mathbf{y}\}\right).\end{aligned} \tag{21}$$

Consequently we can get the minimizer of (16) from the $\{\mathbf{y}_p\}$ that minimize, along with the auxiliary variables $\{\phi_{kp}\}$, the following criterion:

$$\sum_k \sum_p \left|d_{kp}e^{j\phi_{kp}} - \mathbf{a}_{kp}^H\mathbf{y}_p\right|^2. \tag{22}$$

The above criterion can be conveniently minimized (w.r.t $\{\mathbf{y}_p\}$ and $\{\phi_{kp}\}$) by the cyclic algorithm outlined in Table I.

The algorithm in Table I monotonically decreases the criterion (22) at each iteration, and hence it monotonically decreases the original criterion in (16) as well. Thus it is bound to converge to at least a local minimum value of (16). The basic principle of the algorithm is related to the operation of the Sussman-Gerchberg-Saxton Algorithm [20], [21] as described in [22]–[24].

TABLE I
STAGE 1 OF WBFIT

Step 0: Given initial values for $\{\phi_{kp}\}$ (such as $\{\phi_{kp}\}=0$ or $\{\phi_{kp}\}$ randomly generated uniformly in $[0,2\pi]$), repeat the following two steps until convergence (e.g., until the change of $\{\phi_{kp}\}$ in two consecutive iterations is less than a predefined threshold):
Step 1: For $\{\phi_{kp}\}$ set at their latest values (denoted as $\{\hat{\phi}_{kp}\}$), let

$$\mathbf{A}_p=\begin{bmatrix}\mathbf{a}_{1p}^H\\ \vdots\\ \mathbf{a}_{Kp}^H\end{bmatrix},\quad \mathbf{b}_p=\begin{bmatrix}d_{1p}e^{j\hat{\phi}_{1p}}\\ \vdots\\ d_{Kp}e^{j\hat{\phi}_{Kp}}\end{bmatrix} \tag{23}$$

Then (22) can be written as $\sum_p\|\mathbf{b}_p-\mathbf{A}_p\mathbf{y}_p\|^2$. Thus the minimizer $\{\mathbf{y}_p\}$ is given by the least-squares estimate:

$$\hat{\mathbf{y}}_p=(\mathbf{A}_p^H\mathbf{A}_p)^{-1}\mathbf{A}_p^H\mathbf{b}_p,\quad p=-\frac{N}{2},\ldots,0,\ldots,\frac{N}{2}-1. \tag{24}$$

Step 2: For $\{\mathbf{y}_p\}$ set at their latest values, the minimizer $\{\phi_{kp}\}$ is given by (see (21))

$$\hat{\phi}_{kp}=\arg(\mathbf{a}_{kp}^H\hat{\mathbf{y}}_p). \tag{25}$$

*Remark:* It follows from the Parseval equality that the energy-constraint on $\{x_m(n)\}$ [see (18)] imposes the following constraint on $\{\mathbf{y}_p\}$:

$$\sum_{p=-N/2}^{N/2-1}|y_m(p)|^2=N\sum_{n=0}^{N-1}|x_m(n)|^2=N^2,\ \ m=0,\ldots,M-1 \tag{26}$$

where $y_m(p)$ is the $m^{\text{th}}$ element of $\mathbf{y}_p$ [see (13)]. Note that the steps in Table I omit the constraint in (26) for simplicity [observe that this constraint yields a coupling of $\{\mathbf{y}_p\}$, which therefore can no longer be determined separately as in (24)]. Nonetheless, the proposed algorithm performs reasonably well likely because the energy constraint on $\{x_m(n)\}$ is considered in Stage 2 anyway (see below). ■

### B. Stage 2

In Stage 2, we aim to synthesize the waveform $\{\mathbf{x}(n)\}_{n=0}^{N-1}$ under the PAR constraint, so that its DFT approximates the $\{\hat{\mathbf{y}}_p\}_{p=-N/2}^{N/2-1}$ obtained in Stage 1 as closely as possible.

We note first that the $\{\hat{\mathbf{y}}_p\}_{p=-N/2}^{N/2-1}$ obtained in Stage 1 have a phase ambiguity, which can be observed from the minimization criterion in (22): If $(\{\mathbf{y}_p\},\{\phi_{kp}\})$ are minimizers of (22), then $(\{\mathbf{y}_pe^{j\psi_p}\},\{\phi_{kp}+\psi_p\})$ are also minimizers of (22) for any $\psi_p$. In fact, this phase ambiguity results from the original matching problem in (16): $\mathbf{y}_p$ and $\mathbf{y}_pe^{j\psi_p}$ lead to the same value of (16).

To exploit this phase arbitrariness associated with $\{\hat{\mathbf{y}}_p\}$, we introduce auxiliary variables $\{\psi_p\}_{p=-N/2}^{N/2-1}$ and minimize the following fitting criterion w.r.t. both $\{x_m(n)\}$ and $\{\psi_p\}$:

$$\sum_{p=-N/2}^{N/2-1}\left\|\hat{\mathbf{y}}_p^Te^{j\psi_p}-\begin{bmatrix}1 & e^{-j2\pi\frac{p}{N}} & \cdots & e^{-j2\pi\frac{(N-1)p}{N}}\end{bmatrix}\mathbf{X}\right\|^2 \tag{27}$$

TABLE II
STAGE 2 OF WBFIT

Step 0: Given initial values for $\{\psi_p\}$ (such as $\{\psi_p\}=0$), repeat the following two steps until convergence:
Step 1: For $\{\psi_p\}$ fixed at their latest values, the minimization of (30) w.r.t. $\{x_m(n)\}$ depends on the PAR constraint. Under the unit-modulus constraint (i.e., $|x_m(n)|=1$), the minimization of (30) is immediate:

$$\hat{x}_m(n)=\exp(j\arg\{\text{the }(n,m)^{\text{th}}\text{ element of }\mathbf{FS}^T\}),\quad m=0,\ldots,M-1,\ n=0,\ldots,N-1. \tag{31}$$

If instead the PAR $\le\rho$ ($\rho>1$) constraint is imposed, we need to solve $M$ separate minimization problems:

$$\min_{\mathbf{x}_m}\|\mathbf{u}_m-\mathbf{x}_m\|^2\quad(m=0,\ldots,M-1)\quad\text{s.t. PAR}(\mathbf{x}_m)\le\rho \tag{32}$$

where $\mathbf{u}_m$ is the $m^{\text{th}}$ column of $\frac{1}{N}\mathbf{FS}^T$. This problem can be solved efficiently by the "nearest-vector" method proposed in [25] (see also [26]).
Step 2: For $\{x_m(n)\}$ fixed at their most recent values, the minimizer $\{\psi_p\}$ is given by (the derivation of which is similar to (21)):

$$\hat{\psi}_p=\arg\{\hat{\mathbf{y}}_p^H\mathbf{v}_p\},\quad p=-\frac{N}{2},\ldots,\frac{N}{2}-1 \tag{33}$$

where $\mathbf{v}_p^T$ is the $(p+N/2)^{\text{th}}$ row of $\mathbf{F}^H\mathbf{X}$.

where

$$\mathbf{X}=[\mathbf{x}_0\ \mathbf{x}_1\ \cdots\ \mathbf{x}_{M-1}]=\begin{bmatrix}x_0(0) & x_1(0) & \cdots & x_{M-1}(0)\\ \vdots & \vdots & & \vdots\\ x_0(N-1) & x_1(N-1) & & x_{M-1}(N-1)\end{bmatrix}. \tag{28}$$

We further define

$$\mathbf{e}_p^H=\begin{bmatrix}1 & e^{-j2\pi\frac{p}{N}} & \cdots & e^{-j2\pi\frac{(N-1)p}{N}}\end{bmatrix},\quad p=-\frac{N}{2},\ldots,\frac{N}{2}-1$$
$$\mathbf{F}^H=\begin{bmatrix}\mathbf{e}_{-N/2}^H\\ \vdots\\ \mathbf{e}_{N/2-1}^H\end{bmatrix}_{N\times N}$$
$$\mathbf{S}^T=\begin{bmatrix}\hat{\mathbf{y}}_{-N/2}^Te^{j\psi_{-N/2}}\\ \vdots\\ \hat{\mathbf{y}}_{N/2-1}^Te^{j\psi_{N/2-1}}\end{bmatrix}_{N\times M}. \tag{29}$$

Then (27) can be written as

$$\|\mathbf{S}^T-\mathbf{F}^H\mathbf{X}\|^2=N\left\|\frac{1}{N}\mathbf{FS}^T-\mathbf{X}\right\|^2 \tag{30}$$

where the equality comes from the fact that $(1/\sqrt{N})\mathbf{F}$ is a unitary matrix.

Once again we use a cyclic algorithm to minimize (30) (w.r.t. $\{x_m(n)\}$ and $\{\psi_p\}$); see Table II. Note that the required matrix calculation $\mathbf{F}^H\mathbf{X}$ and $\mathbf{FS}^T$ in Table II can be done by fast Fourier transform (FFT) which reduces the computation time.

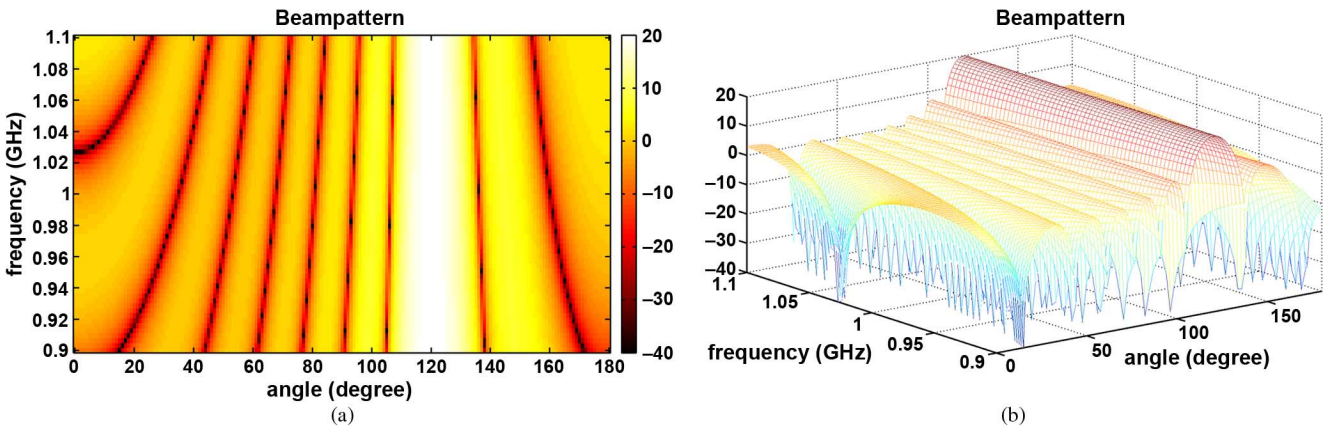


(a) (b)

Fig. 2. The ideal time-delayed beampattern in (35). (a) 2D plot. (b) 3D plot.

It is easy to see that a possible scaling of $\mathbf{S}$ has no effect on (31). The same is true for (32) [which follows from the operation of the method in [25] used to solve (32)]. Therefore, we can choose the desired beampattern $\{d_{kp}\}$ in (22) without any concern for a possible normalization, as $\{\mathbf{y}_p\}$ will automatically scale [see (24)] to fit the chosen $\{d_{kp}\}$ and the scaling of $\{\mathbf{y}_p\}$ does not affect the synthesis of $\{x_m(n)\}$.

To summarize, the proposed two-stage design methodology, first determining $\{\mathbf{y}_p\}$ and then $\{x_m(n)\}$, basically reduces the problem in (22) to the design of $N$ beamforming vectors $\{\mathbf{y}_p\}$, one for each frequency bin and then to matching them by the selection of $\{x_m(n)\}$. Note that there are $2MN$ real-valued elements in $\{\mathbf{y}_p\}$, and $MN$ free variables in $\{x_m(n)\}$ under the unit-modulus constraint, and more than $MN$ degrees of freedom if the PAR is allowed to be larger than 1. In addition, the $\{\psi_p\}$ provide $N$ degrees of freedom. Hence we can expect a "reasonable" performance for the matching step of the proposed approach.

The proposed algorithm is named Wideband Beampattern Formation via Iterative Techniques (WBFIT). Note that the methodology of WBFIT, based on cyclically minimizing the criterion and making use of DFT, is similar to that of the CAN algorithm which was proposed in [27], [28] to design a single sequence or a set of sequences with good correlation properties. Although WBFIT relies on an iterative process, the updating formulas are relatively simple and the iteration turns out to converge very fast. For every numerical example shown in the next section, the execution of the WBFIT algorithm in MATLAB takes only a few seconds on an ordinary PC.

## IV. Numerical Examples

Unless stated otherwise, the following setting is used in this section: a ULA of $M = 10$ elements, the carrier frequency of the transmitted signal is $f_c = 1$ GHz, the bandwidth is $B = 200$ MHz and the number of symbols is $N = 64$. The symbol period is $T_s = 1/B$. The inter-element spacing is given by $d = c/2(f_c + B/2)$, that is, half wavelength of the highest in-band frequency to avoid grating lobes. The spatial angle is divided into $K = 180$ grid points (i.e., one degree per grid step).

*Remark:* In practical applications the antenna elements of an array are typically mutually coupled. The interelement spacing $d$ chosen above results in oversampling (i.e. sampling interval less than half wavelength) for lower in-band frequencies and may render the mutual coupling effects nonnegligible, which could lead to energy being coupled into transmitters. However, this issue lies outside the scope of this paper (as it depends more on the specific hardware implementation such as the system tolerance and antenna types), and we refer interested readers to, e.g., [29]–[31] for relevant discussions on decoupling. ■

### A. The Ideal Time-Delayed Case

It follows from (6) that we can steer the transmit beam towards the angle $\theta_0$ by choosing the following signal spectrum:

$$\mathbf{y}(f) = \sqrt{N}\mathbf{a}(\theta_0, f), \quad f \in \left[-\frac{B}{2}, \frac{B}{2}\right] \tag{34}$$

where $\sqrt{N}$ is due to the energy constraint. Equation (34) leads to [see (15)]

$$P_{kp} = N\left|\sum_{m=0}^{M-1} e^{j2\pi\left(\frac{p}{NT_s}+f_c\right)\frac{md(\cos\theta_0-\cos\theta_k)}{c}}\right|^2 \tag{35}$$

where for a fixed value of $f$ (i.e., $p$), the beam is steered in the direction of $\theta_0$ as in the case of a classic (narrowband) phased array. The underlying signals, i.e., the inverse Fourier transform of (34), are given by (up to a multiplicative constant)

$$x_m(t) = \mathrm{sinc}\left(\frac{\pi}{T_s}\left(t - \frac{md\cos\theta_0}{c}\right)\right), \quad m = 0, \ldots, M-1 \tag{36}$$

where $\mathrm{sinc}(t) = \sin(x)/x$. Note that such an $\{x_m(t)\}$ has a very high PAR which is highly undesired. Moreover, because $d/c = 1/(2f_c + B) \ll T_s$, the required time delay $md\cos\theta_0/c$ can be too small to be really implemented in practice, especially when $\theta_0$ is close but not equal to 90°.

We show the beampattern $10\lg(P_{kp}/N)$ for $\theta_0 = 120°$ as a 2D plot in Fig. 2(a), as well as a 3D plot in Fig. 2(b). The beampattern exhibits a clean mainlobe at $\theta_0$ across the entire frequency range.

*Remark:* In the narrowband case, given the same antenna aperture the transmit beampattern generated by a phased array has the smallest mainlobe width. In the above example, we use the unrealistically time-delayed $\{x_m(t)\}$ in (36) to get

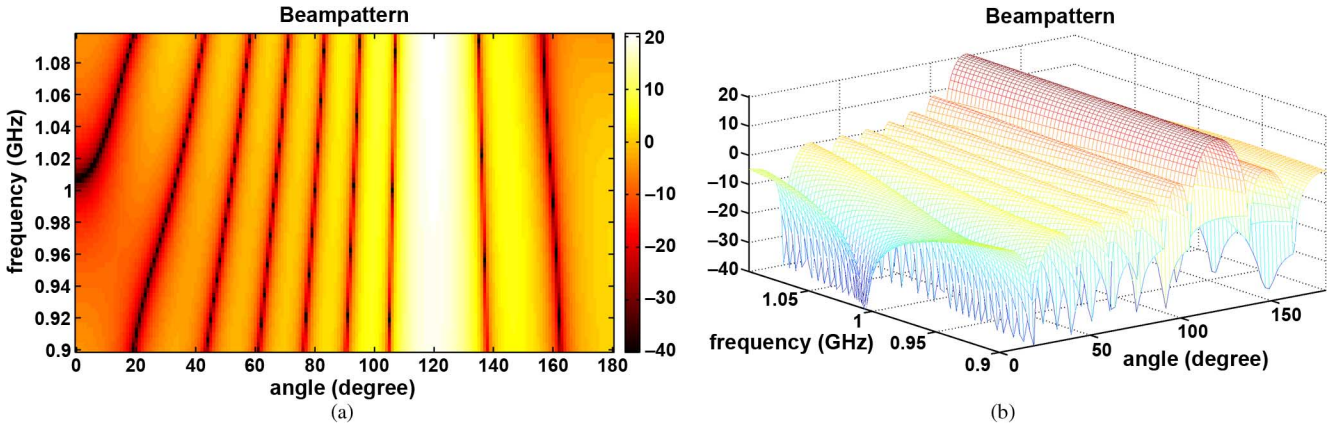


(a) (b)

Fig. 3. The WBFIT beampattern under only the total energy constraint. The desired beampattern is given in (37). (a) 2D plot. (b) 3D plot.

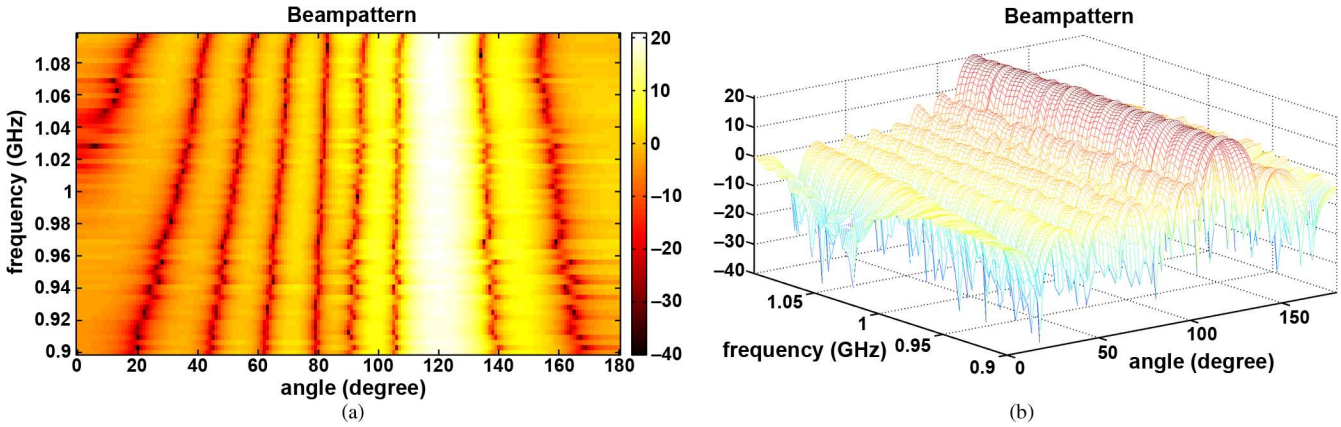


(a) (b)

Fig. 4. The WBFIT beampattern under the unit-modulus constraint. The desired beampattern is given in (37). (a) 2D plot. (b) 3D plot.

the phased array-like beampattern in (35), which thus has the narrowest mainlobe for every fixed frequency. Therefore, we call it the "ideal time-delayed" case.

It has been assumed that for each array element the energy $N$ is emitted in all directions; and the energy constraint $\sum_p |y_m(p)|^2 = N^2$ in (26) indicates that on average $|y_m(p)|^2$ equals $N$. Therefore, were there only one array element, $P_{kp}$ would equal $N$ at every grid point in the angle-frequency plane [see, e.g., (35)]. This is the reason why the normalization $10\lg(P_{kp}/N)$ is used in all plots. Now that there are $M$ transmit waveforms, the coherent sum gives $\max P_{kp} = \max |\mathbf{a}_{kp}^H \mathbf{y}_p|^2 = |M\sqrt{N}|^2 = M^2 N$, which leads to $10\lg(M^2N/N) = 20$ dB in the plot. In fact, in the above ideal time-delayed case, all $M$ waveforms add coherently at $\theta = \theta_0$ and the energy is evenly distributed at $\theta = \theta_0$ for all frequencies, which produces a constant 20 dB mainlobe height [see Fig. 2 and (35)]. In other examples, however, the mainlobe height is not necessarily 20 dB and the upper limit of the colorbar always corresponds to the largest value in the plot. ■

### *B. WBFIT—Example 1*

We use the proposed WBFIT algorithm to synthesize the following desired transmit beampattern:

$$d(\theta, f+f_c) = \begin{cases} 1, & \theta = 120^\circ \\ 0, & \text{other } \theta \end{cases} \quad \text{for all } f \in \left[-\frac{B}{2}, \frac{B}{2}\right] \quad (37)$$

that is, a beampattern with the mainlobe (as narrow as possible) located at 120° across the frequency support.

Stage 1 of WBFIT generates the DFT vectors $\{\hat{\mathbf{y}}_p\}_{p=-N/2}^{N/2-1}$, which are further normalized to preserve the total energy (i.e., normalized such that $\sum_p |\mathbf{y}_p|^2 = MN^2$). Fig. 3 shows the beampattern $P_{kp}$ that is calculated directly from these $\{\hat{\mathbf{y}}_p\}$. The so-obtained beampattern is quite similar to the ideal one in Fig. 2. However, the underlying waveforms corresponding to Fig. 3, given by the inverse DFT (IDFT) of $\{\hat{\mathbf{y}}_p\}_{p=-N/2}^{N/2-1}$, do not satisfy the energy and PAR requirement. Indeed, the $M$ sequences obtained from the IDFT of $\{\hat{\mathbf{y}}_p\}$ have energies varying from 55.4 to 71.2 and have PARs varying from 1.3 to 1.8. Note that such transmit sequences need to be scaled in practice so that the maximum power/energy does not exceed the system specifications, which will inevitably result in an energy loss (i.e., the value of the beampattern is lowered).

We then proceed to Stage 2 of WBFIT and synthesize sequences $\{\hat{x}_m(n)\}$ under the unit-modulus constraint. After that, we compute the DFT of $\{\hat{x}_m(n)\}$ and obtain the beampattern using (15); see Fig. 4. It is apparent that the strict unit-modulus constraint degrades the beampattern matching. Table III shows the value of the obtained minimization criterion [see (16)] associated with Figs. 3 and 4, respectively.

Next we examine the beampattern of the continuous waveforms (see the last *Remark* in Section III) corresponding to the so-obtained $\{\hat{x}_m(n)\}$. More specifically, we pass each

TABLE III
MINIMIZATION CRITERION FOR FIGS. 3 AND 4

| | Fig. 3 | Fig. 4 |
|---|---|---|
| Criterion in (16) | 5987914 | 6048430 |

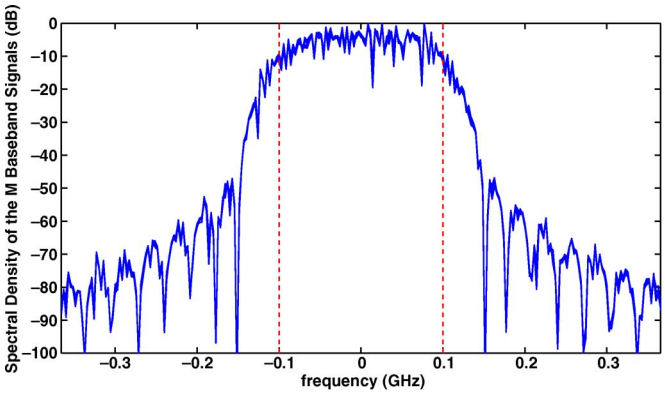


Fig. 5. The overlaid spectral densities of the continuous waveforms corresponding to the sequences used in Fig. 4. The two vertical dotted lines represent the boundaries of the frequency range of interest.

$\{\hat{x}_m(n)\}_{n=0}^{N-1}$ $(m = 0, \ldots, M-1)$ through an FIR raised-cosine filter (with the roll-off factor equal to 0.5) to get the continuous signal $\hat{x}_m(t)$. The spectral density functions of $\{\hat{x}_m(t)\}$ are shown in Fig. 5 in an overlapped manner, from which we observe that the spectrum is well contained within $[f_c - B/2, f_c + B/2]$ despite of a certain leakage outside the frequency range of interest. The beampattern of $\{\hat{x}_m(t)\}$, as defined in (6), is shown in Fig. 6. Compared to Fig. 4, the beampattern becomes more raspy and the mainlobe becomes relatively blurred. As discussed in the *Remark* at the end of Section II, a practical pulse shaping renders (6) and (15) not exactly equivalent. Since the WBFIT algorithm only aims to match (15) to the desired beampattern, the nonequivalence between (6) and (15) explains the degradation from Fig. 4to Fig. 6. Note that we can choose a $T_s$ smaller than $1/B$ to achieve a better spectral containment; however the improvement of the resulting beampattern matching is limited and thus the related plots are not shown for the sake of conciseness.

### C. WBFIT—Example 2

In this example we consider the following desired beampattern:

$$d(\theta, f + f_c) = \begin{cases} 1, & f_c - B/2 \le f \le f_c \text{ and } \theta = 120^\circ \\ 1, & f_c \le f \le f_c + B/2 \text{ and } \theta = 60^\circ \\ 0, & \text{elsewhere.} \end{cases} \tag{38}$$

The WBFIT beampattern under the unit-modulus constraint is shown in Fig. 7 and that under the $\mathrm{PAR} \le 2$ constraint is shown in Fig. 8. While Fig. 7 already provides a reasonably good beampattern matching, relaxing the PAR from 1 to 2 leads to the visibly better result in Fig. 8 due to more degrees of freedom in waveform generation. Table IV shows this performance improvement in terms of the minimization criterion.

### D. WBFIT—Example 3

In both examples above, we focused on achieving a beampattern with mainlobe(s) as narrow as possible. Particularly the ideal phased array-like beampattern in Fig. 2, which has the narrowest possible mainlobe, was well approximated by using practical waveforms in Section IV-B. If we want to obtain a narrower mainlobe, we have to use a larger value of $M$, i.e., more transmit antenna elements.

Here we instead consider the following beampattern with a wider mainlobe:

$$d(\theta, f + f_c) = \begin{cases} 1, & 100^\circ \le \theta \le 140^\circ \\ 0, & \text{other } \theta \end{cases} \quad \text{for all } f \in \left[-\frac{B}{2}, \frac{B}{2}\right]. \tag{39}$$

The obtained WBFIT beampattern under the unit-modulus constraint is shown in Fig. 9 and that under the $\mathrm{PAR} \le 2$ constraint is shown in Fig. 10. We observe that the mainlobe in Figs. 9 or 10 has an almost constant width for different frequencies, unlike the mainlobe in Fig. 2 whose width tends to shrink as the frequency increases (the well-known beam squint phenomenon). Also note the "mainlobe splitting" in Figs. 9 or 10. Had we synthesized an even wider mainlobe than (39), the splitting would be more severe (e.g., the mainlobe can split twice and there are three local maxima in the mainlobe area).

In all above examples the bandwidth $B$ was set to 200 MHz. A larger bandwidth means more constraints and thus the beampattern matching is expected to be more difficult. To illustrate, we repeat the example corresponding to Fig. 4 except that the bandwidth is changed to 350 MHz. The result is shown in Fig. 11, where the beampattern becomes more irregular than in Fig. 4.

Regarding choosing $N$ (the number of transmitted symbols), we note that increasing $N$ does not necessarily lead to a better beampattern matching. The reason is that while a larger $N$ increases the degrees of freedom of the waveform $\{x_m(n)\}$, it also increases proportionally the number of elements in $\{\mathbf{y}_p\}$ that are to be matched in Stage 2 of WBFIT (cf. the discussion at the end of Section III). However, $N$ cannot be made too small because the frequency grid should be dense enough to cover the frequency support finely.

We finally point out that the initialization of WBFIT (i.e., Step 0 in both Stages) does not play an important role in the algorithm performance. In all numerical examples presented, randomly generated phases are used in the initialization; different initializations lead to different waveforms but all of these waveforms have similar beampatterns. This also signifies the fact that the beampattern matching problem is highly multimodal (thus a difficult problem).

## V. CONCLUDING REMARKS

In this paper we have proposed a new algorithm named WBFIT to synthesize transmit beampatterns for wideband MIMO systems. The waveform diversity in MIMO systems (i.e., independent waveforms from different array elements) is exploited so as to synthesize various types of wideband beampatterns. At the same time, practical waveform constraints such as unit-modulus or low PAR are taken into account. The WBFIT algorithm adopts a cyclic approach to minimize the beampattern matching criterion, it is computationally efficient

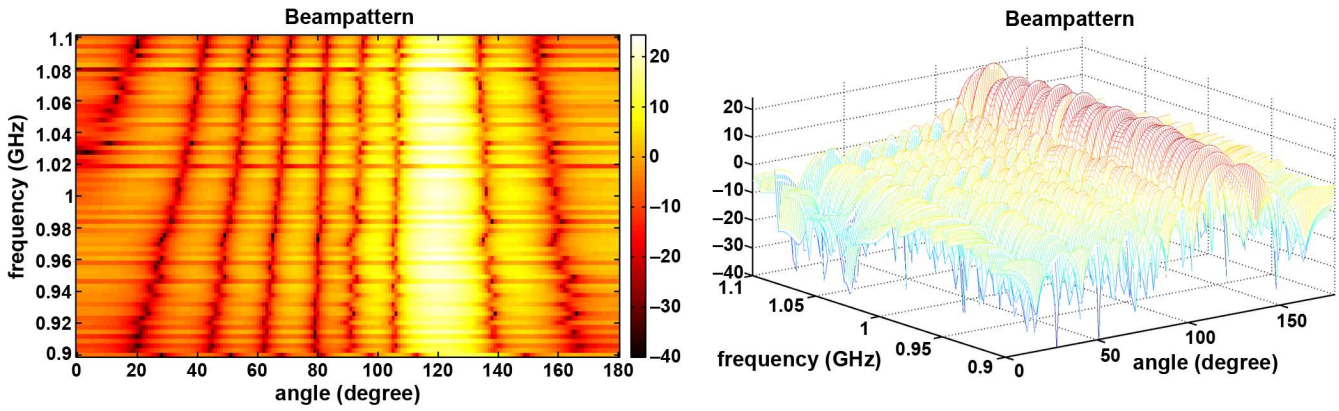


(a) (b)

Fig. 6. The WBFIT beampattern of the continuous waveforms corresponding to the sequences used in Fig. 4. The desired beampattern is given in (37). (a) 2D plot. (b) 3D plot.

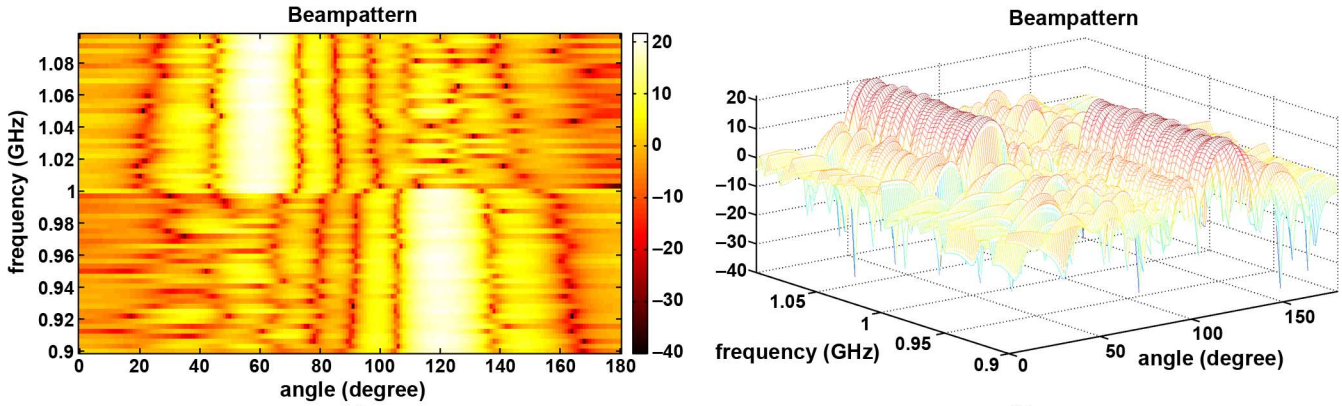


(a) (b)

Fig. 7. The WBFIT beampattern under the unit-modulus constraint. The desired beampattern is given in (38). (a) 2D plot. (b) 3D plot.

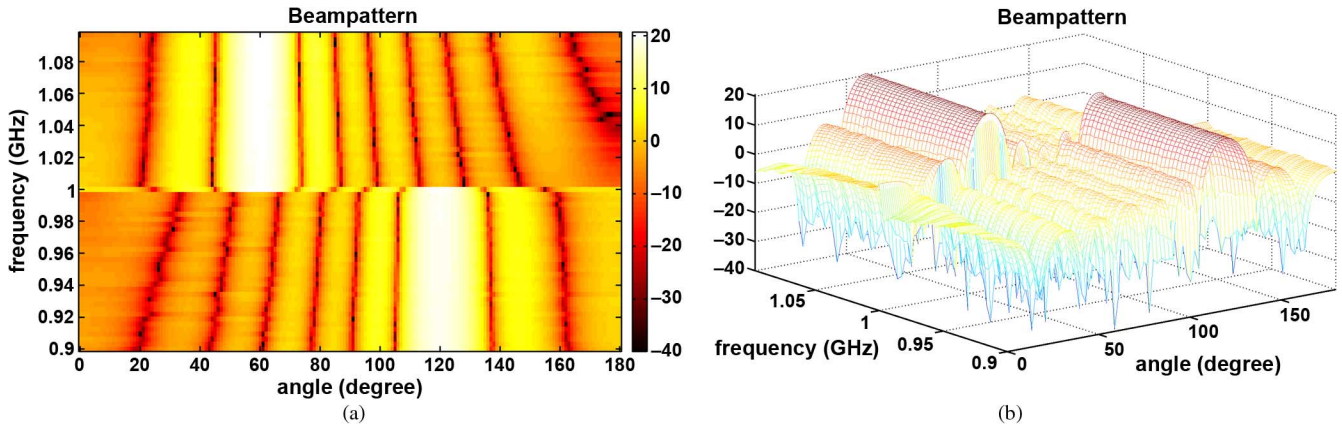


(a) (b)

Fig. 8. The WBFIT beampattern under the $\mathrm{PAR} \leq 2$ constraint. The desired beampattern is given in (38). (a) 2D plot. (b) 3D plot.

TABLE IV
MINIMIZATION CRITERION FOR FIGS. 7 AND 8

| | Fig. 7 | Fig. 8 |
|---|---|---|
| Criterion in (16) | 5706841 | 5619877 |

and its local convergence is guaranteed. Several numerical examples have been included to demonstrate the effectiveness of WBFIT in generating practical waveforms to match a desired beampattern.

WBFIT was derived under the setting of 1D ULA (see Fig. 1) and it can be adapted to the 1D non-ULA case by using a more general steering vector than the one in (7); see, e.g., [17]. For 2D arrays, the optimization problem becomes harder due to the increased spatial dimension. Extensions to such arrays are left for future work.

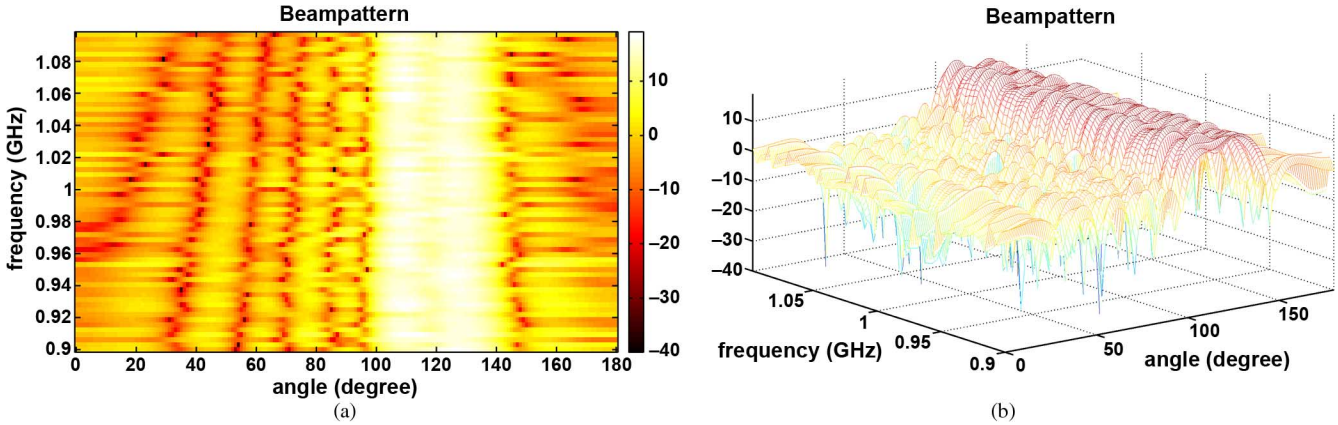


(a) (b)

Fig. 9. The WBFIT beampattern under the unit-modulus constraint. The desired beampattern is given in (39). (a) 2D plot. (b) 3D plot.

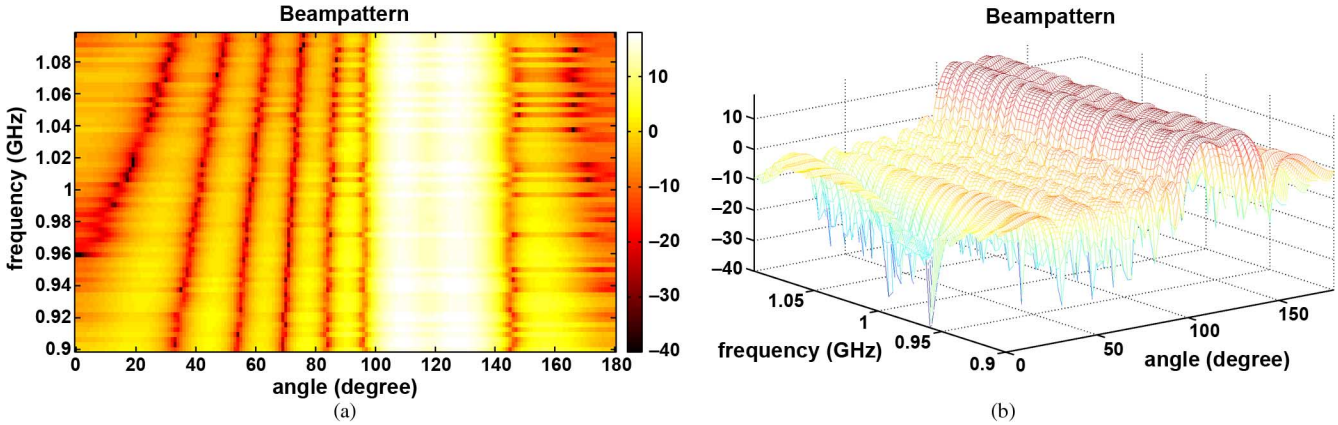


(a) (b)

Fig. 10. The WBFIT beampattern under the $\mathrm{PAR} \leq 2$ constraint. The desired beampattern is given in (39). (a) 2D plot. (b) 3D plot.

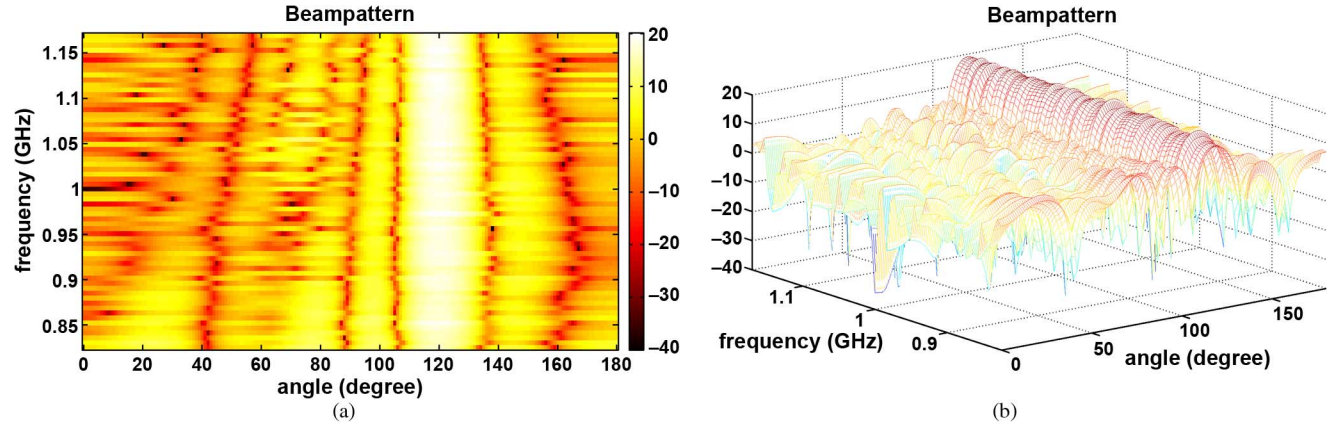


(a) (b)

Fig. 11. The WBFIT beampattern with all settings the same as those used in Fig. 4, except that the bandwidth $B$ is changed from 200 to 350 MHz. (a) 2D plot. (b) 3D plot.

## Appendix A
## Narrowband Transmit Beampattern

In the narrowband case, $B \ll f_c$ and therefore the distribution of energy versus frequency $f$ is of less interest. Instead, the total energy over $f$ is the quality of interest, which is given by [see (15)]

$$P(\theta_k) = \sum_{p=-N/2}^{N/2-1} P_{kp} = \sum_{p=-N/2}^{N/2-1} \left|\mathbf{a}_{kp}^H \mathbf{y}_p\right|^2. \qquad (40)$$

Since the interelement spacing $d$ is on the order of the carrier wavelength, the narrowband assumption $B \ll f_c$ implies that $(fd\cos\theta/c) \sim 0$ $(-B/2 \leq f \leq B/2)$, which means that the steering vector $\mathbf{a}_{kp}$ is independent of frequency. Thus its subscript $p$ can be dropped and (40) becomes

$$\begin{aligned} P(\theta_k) &= \mathbf{a}_k^H \left[\sum_{p=-N/2}^{N/2-1} \mathbf{y}_p \mathbf{y}_p^H\right] \mathbf{a}_k \\ &= \mathbf{a}_k^H \left[\sum_{u=0}^{N-1}\sum_{v=0}^{N-1} \mathbf{x}(u)\mathbf{x}^H(v) \left(\sum_{p=-N/2}^{N/2-1} e^{-j2\pi\frac{(u-v)p}{N}}\right)\right] \mathbf{a}_k \\ &= \mathbf{a}_k^H \left[N \sum_{n=0}^{N-1} \mathbf{x}(n)\mathbf{x}^H(n)\right] \mathbf{a}_k \qquad (41) \end{aligned}$$

where $\mathbf{x}(n)$ is defined in (14). The result in (41), up to a multiplicative constant, coincides with the narrowband beampattern expression used in [14].

## APPENDIX B
## RECEIVE BEAMPATTERN

Paralleling the discussions in Section II, we briefly formulate here the receive beampattern synthesis problem for wideband signals.

Suppose that a wideband signal $g(t)e^{j2\pi f_c t}$ with frequency band $[f_c - B/2, f_c + B/2]$ is impinging from angle $\theta$ ($0^\circ \leq \theta \leq 180^\circ$) on a ULA. Let $G(f)$ denote the Fourier transform of $g(t)$. The signal received at the $m^{\text{th}}$ array element can be written as

$$\begin{aligned} r_m(t) &= g\left(t - \frac{md\cos\theta}{c}\right) e^{j2\pi f_c\left(t - \frac{md\cos\theta}{c}\right)} \\ &= \int_{-B/2}^{B/2} G(f) e^{-j2\pi(f+f_c)\frac{md\cos\theta}{c}} e^{j2\pi(f+f_c)t}\, df. \end{aligned} \quad (42)$$

Let $H_m(f)$ denote the frequency response of the FIR filter used to process $r_m(t)$. Then the receive beampattern can be expressed as

$$A(\theta, f+f_c) = \left|\sum_{m=0}^{M-1} H_m(f) e^{-j2\pi(f+f_c)\frac{md\cos\theta}{c}}\right|^2 \quad f \in \left[-\frac{B}{2}, \frac{B}{2}\right] \quad (43)$$

where $G(f)$ is omitted because it is the same for all array elements. The receive beampattern synthesis problem can be stated as designing a set of $M$ filters $\{h_m(t)\}_{m=0}^{M-1}$ (the Fourier transform of $h_m(t)$ is given by $H_m(f)$) such that $A(\theta, f+f_c)$ matches a desired pattern.

As pointed out in the Introduction, there is no essential constraint on $\{h_m(t)\}_{m=0}^{M-1}$, the design of which can, therefore, be done by many approaches, such as classic filter design methods [4] or convex optimization [6]. The transmit beampattern design, which is the topic of this paper, turns out to be much harder because of the PAR constraint, despite the fact that (6) and (43) have the same form.

## REFERENCES


[1] R. J. Mailloux, "Phased array theory and technology," *Proc. IEEE*, vol. 70, no. 3, pp. 246–291, Mar. 1982.

[2] C. Dolph, "A current distribution for broadside arrays which optimizes the relationship between beam width and side-lobe level," *Proc. IRE*, vol. 34, no. 6, pp. 335–348, Jun. 1946.

[3] R. Elliott, "Design of line source antennas for narrow beamwidth and asymmetric low sidelobes," *IEEE Trans. Antennas Propag.*, vol. 23, no. 1, pp. 100–107, Jan. 1975.

[4] D. B. Ward, R. A. Kennedy, and R. C. Williamson, "FIR filter design for frequency invariant beamformers," *IEEE Signal Process. Lett.*, vol. 3, no. 3, pp. 69–71, Mar. 1996.

[5] H. L. Van Trees, *Optimum Array Processing: Part IV of Detection, Estimation, and Modulation Theory*. New York: Wiley, 2002.

[6] H. Lebret and S. Boyd, "Antenna array pattern synthesis via convex optimization," *IEEE Trans. Signal Process.*, vol. 45, no. 3, pp. 526–532, Mar. 1997.

[7] D. P. Scholnik and J. O. Coleman, "Optimal design of wideband array patterns," presented at the IEEE Int. Radar Conf., Washington DC, May 2000.

[8] G. Cardone, G. Cincotti, and M. Pappalardo, "Design of wide-band arrays for low side-lobe level beam patterns by simulated annealing," *IEEE Trans. Ultrason., Ferroelectr., Freq. Control*, vol. 49, no. 8, Aug. 2002.

[9] G. San Antonio and D. R. Fuhrmann, "Beampattern synthesis for wideband MIMO radar systems," in *Proc. 1st IEEE Int. Workshop Computational Advances Multi-Sensor Adaptive Processing*, Puerto Vallarta, Mexico, Dec. 13–15, 2005, pp. 105–108.

[10] J. Li, Y. Xie, P. Stoica, X. Zheng, and J. Ward, "Beampattern synthesis via a matrix approach for signal power estimation," *IEEE Trans. Signal Process.*, vol. 55, no. 12, pp. 5643–5657, Dec. 2007.

[11] M. I. Skolnik, *Radar Handbook, Second Edition*. New York: McGraw-Hill, 1990.

[12] L. K. Patton and B. D. Rigling, "Modulus constraints in adaptive radar waveform design," presented at the IEEE Radar Conf., Rome, Italy, May 2008.

[13] K. W. Forsythe and D. W. Bliss, "Waveform correlation and optimization issues for MIMO radar," in *Proc. 39th Asilomar Conf. Signals, Systems, Computers*, Pacific Grove, CA, Nov. 2005, pp. 1306–1310.

[14] P. Stoica, J. Li, and Y. Xie, "On probing signal design for MIMO radar," *IEEE Trans. Signal Process.*, vol. 55, no. 8, pp. 4151–4161, Aug. 2007.

[15] D. R. Fuhrmann and G. San Antonio, "Transmit beamforming for MIMO radar systems using signal cross-correlation," *IEEE Trans. Aerosp. Electron. Syst.*, vol. 44, no. 1, pp. 1–16, Jan. 2008.

[16] P. Stoica, J. Li, and X. Zhu, "Waveform synthesis for diversity-based transmit beampattern design," *IEEE Trans. Signal Process.*, vol. 56, no. 6, pp. 2593–2598, Jun. 2008.

[17] B. Guo and J. Li, "Waveform diversity based ultrasound system for hyperthermia treatment of breast cancer," *IEEE Trans. Biomed. Eng.*, vol. 55, no. 2, pp. 822–826, Feb. 2008.

[18] N. Levanon and E. Mozeson, *Radar Signals*. New York: Wiley, 2004.

[19] J. G. Proakis, *Digital Communications*, 4th ed. New York: McGraw-Hill, 2001.

[20] S. Sussman, "Least-square synthesis of radar ambiguity functions," *IEEE Trans. Inf. Theory*, vol. 8, no. 3, pp. 246–254, 1962.

[21] R. Gerchberg and W. Saxton, "Phase determination for image and diffraction plane pictures in the electron microscope," *Optik (Stuttgart)*, vol. 34, no. 3, pp. 275–284, 1971.

[22] J. R. Fienup, "Phase retrieval algorithms: A comparison," *Appl. Opt.*, vol. 21, no. 15, pp. 2758–2769, Feb. 1982.

[23] A. Weiss and J. Picard, "Maximum-likelihood position estimation of network nodes using range measurements," *IET Signal Process.*, vol. 2, no. 4, pp. 394–404, 2008.

[24] W. Roberts, H. He, J. Li, and P. Stoica, "Probing waveform synthesis and receiver filter design," *IEEE Signal Process. Mag.*, vol. 27, no. 4, pp. 99–112, Jul. 2010.

[25] J. A. Tropp, I. S. Dhillon, R. W. Heath, and T. Strohmer, "Designing structured tight frames via an alternating projection method," *IEEE Trans. Inf. Theory*, vol. 51, no. 1, pp. 188–209, Jan. 2005.

[26] H. He, P. Stoica, and J. Li, "On aperiodic-correlation bounds," *IEEE Signal Process. Lett.*, vol. 17, no. 3, pp. 253–256, Mar. 2010.

[27] P. Stoica, H. He, and J. Li, "New algorithms for designing unimodular sequences with good correlation properties," *IEEE Trans. Signal Process.*, vol. 57, no. 4, pp. 1415–1425, Apr. 2009.

[28] H. He, P. Stoica, and J. Li, "Designing unimodular sequence sets with good correlations-Including an application to MIMO radar," *IEEE Trans. Signal Process.*, vol. 57, no. 11, pp. 4391–4405, Nov. 2009.

[29] H. T. Hui, "Decoupling methods for the mutual coupling effect in antenna arrays: A review," *Recent Patents Eng.*, vol. 1, no. 2, pp. 187–193, 2007.

[30] G. Frazer, Y. Abramovich, and B. Johnson, "Spatially waveform diverse radar: Perspectives for high frequency OTHR," in *Proc. IEEE Radar Conf.*, Boston, MA, Jun. 2007, pp. 385–390.

[31] T. Svantesson, "Modeling and estimation of mutual coupling in a uniform linear array of dipoles," presented at the 1999 IEEE Int.Conf. Acoustics, Speech, Signal Processing, Phoenix, AZ, Mar. 1999.

**Hao He** (S'08) received the B.Sc. degree from the University of Science and Technology of China (USTC), Hefei, in 2007, and the M.Sc. degree from the University of Florida, Gainesville, in 2009, both in electrical engineering.

He is currently pursuing the Ph.D. degree with the Department of Electrical and Computer Engineering, University of Florida, Gainesville. His research interests are in the areas of radar/sonar waveform design and spectral estimation.

**Petre Stoica** (F'94) received the D.Sc. degree in automatic control from Polytechnic Institute of Bucharest (BPI), Bucharest, Romania, in 1979 and an honorary doctorate degree in science from Uppsala University (UU), Uppsala, Sweden, in 1993.

He is a professor of systems modeling with the Division of Systems and Control, Department of Information Technology, UU. Previously, he was a professor of system identification and signal processing with the Faculty of Automatic Control and Computers at BPI. He held longer visiting positions with Eindhoven University of Technology, Eindhoven, The Netherlands; Chalmers University of Technology, Gothenburg, Sweden (where he held a Jubilee Visiting Professorship); UU; the University of Florida, Gainesville; and Stanford University, Stanford, CA. His main scientific interests are in the areas of system identification, time series analysis and prediction, statistical signal and array processing, spectral analysis, wireless communications, and radar signal processing. He has published nine books, 10 book chapters, and some 500 papers in archival journals and conference records. The most recent book he coauthored, with R. Moses, is *Spectral Analysis of Signals* (Englewood Cliffs, NJ: Prentice-Hall, 2005).

Dr. Stoica is on the editorial boards of six journals: the *Journal of Forecasting*; *Signal Processing*; *Circuits, Signals, and Signal Processing*; *Digital Signal Processing: A Review Journal*; *Signal Processing Magazine*; and *Multidimensional Systems and Signal Processing*. He was a co-guest editor for several special issues on system identification, signal processing, spectral analysis, and radar for some of the aforementioned journals, as well as for the IEE PROCEEDINGS. He was corecipient of the IEEE ASSP Senior Award for a paper on statistical aspects of array signal processing. He was also recipient of the Technical Achievement Award of the IEEE Signal Processing Society. In 1998, he was the recipient of a Senior Individual Grant Award of the Swedish Foundation for Strategic Research. He was also co-recipient of the 1998 EURASIP Best Paper Award for Signal Processing for a work on parameter estimation of exponential signals with time-varying amplitude, a 1999 IEEE Signal Processing Society Best Paper Award for a paper on parameter and rank estimation of reduced-rank regression, a 2000 IEEE Third Millennium Medal, and the 2000 W. R. G. Baker Prize Paper Award for a paper on maximum likelihood methods for radar. He was a member of the international program committees of many topical conferences. From 1981 to 1986, he was a Director of the International Time-Series Analysis and Forecasting Society, and he was also a member of the IFAC Technical Committee on Modeling, Identification, and Signal Processing. He is also a member of the Royal Swedish Academy of Engineering Sciences, an honorary member of the Romanian Academy, and a fellow of the Royal Statistical Society.

**Jian Li** (S'87–M'91–SM'97–F'05) received the M.Sc. and Ph.D. degrees in electrical engineering from Ohio State University, Columbus, in 1987 and 1991, respectively.

From April 1991 to June 1991, she was an Adjunct Assistant Professor with the Department of Electrical Engineering, Ohio State University. From July 1991 to June 1993, she was an Assistant Professor with the Department of Electrical Engineering, University of Kentucky, Lexington. Since August 1993, she has been with the Department of Electrical and Computer Engineering, University of Florida, Gainesville, where she is currently a Professor. In fall 2007, she was on sabbatical leave at MIT, Cambridge. Her current research interests include spectral estimation, statistical and array signal processing, and their applications.

Dr. Li is a Fellow of IET. She is a member of Sigma Xi and Phi Kappa Phi. She received the 1994 National Science Foundation Young Investigator Award and the 1996 Office of Naval Research Young Investigator Award. She was an Executive Committee Member of the 2002 International Conference on Acoustics, Speech, and Signal Processing, Orlando, Florida, May 2002. She was an Associate Editor of the IEEE TRANSACTIONS ON SIGNAL PROCESSING from 1999 to 2005, an Associate Editor of the IEEE SIGNAL PROCESSING MAGAZINE from 2003 to 2005, and a member of the Editorial Board of *Signal Processing*, a publication of the European Association for Signal Processing (EURASIP), from 2005 to 2007. She has been a member of the Editorial Board of *Digital Signal Processing—A Review Journal*, a publication of Elsevier, since 2006. She is presently a member of the Sensor Array and Multichannel (SAM) Technical Committee of the IEEE Signal Processing Society. She is a coauthor of the papers that have received the First and Second Place Best Student Paper Awards, respectively, at the 2005 and 2007 Annual Asilomar Conferences on Signals, Systems, and Computers in Pacific Grove, CA. She is also a coauthor of the paper that has received the M. Barry Carlton Award for the best paper published in IEEE TRANSACTIONS ON AEROSPACE AND ELECTRONIC SYSTEMS in 2005.